Australian Meteorological and Oceanographic Journal 62 (2012) 117–126

Pyrocumulonimbus pair in Wollemi and Blue Mountains National Parks, 22 November 2006

M.D. Fromm[1], R.H.D. McRae[2], J.J. Sharples[3], G.P. Kablick III[1]
[1]Naval Research Laboratory, USA
[2]ACT Emergency Services Agency, Australia
[3]Applied and Industrial Mathematics Research Group,
School of Physical, Environmental and Mathematical Sciences
University of New South Wales, Australia

(Manuscript received March 2012; revised August 2012)

On 22 November 2006 a pair of pyrocumulonimbus (pyroCb) storms, roughly 75 km apart, erupted simultaneously in the forests of Wollemi and Blue Mountains National Parks. The so-named Wollemi and Grose Valley fires blew up at an unusual time—late morning—and injected smoke into the uppermost troposphere. This is the first pyroCb event recorded during active pyroconvection by NASA's A-Train satellite constellation. Hence we show for the first time the pyroconvection column from simultaneous passive imagers, active lidar and radar, and UV backscattering instruments. There are no previous reports of pyroCb activity from Wollemi, and a report of the Grose Valley pyroconvective column limited its vertical extent to 6 km. Here we show, using ground-based radar data, that both fires blew up quasi-simultaneously before local noon. The Grose Valley pyroCb penetrated to the tropopause, the Wollemi pyroCb injection height exceeded the tropopause by 1–3 km. Analysis of a portion of the smoke plume sampled by the A-Train on 23 November confirms tropopause injection altitude. We explore a variety of meteorological observations and analyses to determine that the blow ups on 22 November 2006 (and only on this date in the fires' lifetimes) were mostly a consequence of anomalous boundary layer warmth and wind speed.

Introduction

The Australian spring and summer of 2006–2007 was punctuated by a number of bushfire events that had notable impact on landscapes, communities and the atmosphere. For example, Victorian bushfires in mid-December 2006 blew up and injected a smoke pall that circled the globe (Dirksen et al., 2009). Mills and McCaw (2010) catalogued and explored several extreme or unexpected bushfire events between September 2006 and January 2007. Many of their cases involved pyroconvection manifested as so-called pyrocumulonimbus (pyroCb for short), firestorms with sufficient vertical extent to involve ice (and hail) formation, lightning, and a resultant plume in the upper troposphere or lower stratosphere (Fromm et al., 2006). A deeper exploration of such pyroCb events is needed to shed light on the extreme weather/fuel/fire conditions that trigger such overtly destructive storms. During the Australian 2006–2007 season, there were at least two blow up events that were incompletely characterised and require a more detailed examination. One of these is the Dirksen et al. (2009) case, which is under development. Here we will analyse two pyroCbs that occurred on 22 November 2006 in the east central forests of New South Wales (Fig. 1). Our study was motivated by the fortuitous sampling of an active pyrocumulonimbus anvil from one pyroCb, and the detrained anvil from the second by satellite-based cloud radar and lidar. These and other satellite views significantly expand our understanding of the strength of the firestorms and their atmospheric impact. Fortunately there is a wealth of ground- and aircraft-based data of both blow ups to reconcile with the satellite views, and to clarify the fire energy pulses associated with the deep pyroconvection.

Corresponding author address: Mike Fromm, Naval Research Laboratory, USA.
Email: mike.fromm@nrl.navy.mil

Data

Satellite

This case study was motivated by the fact that the pyroconvection in New South Wales on 22 November 2006 was captured by NASA's A-Train fleet of quasi-simultaneous passive and active sensors passing over the fire zone nominally at 1330 local standard time (Stephens et al., 2002). Here we utilise four A-Train sensors, the MODerate-resolution Imaging Spectroradiometer (MODIS) (King et al., 1992) onboard the Aqua satellite, the Ozone Monitoring Instrument (OMI) onboard Aura, the Cloud-Aerosol Lidar with Orthogonal Polarization (CALIOP) onboard the Cloud-Aerosol Lidar and Infrared Pathfinder Satellite Observations (CALIPSO) satellite, and the CloudSat cloud profiling radar.

The MODIS data include level 1b true colour imagery, 11 μm brightness temperature, and level two fire hot spot detections (Giglio et al., 2003). The hot spot data are a prime input to the construction of fire perimeters shown in our analysis. The OMI data are level two absorbing aerosol index (AI) (Torres et al., 2007). The AI is strategic for identifying smoke plumes in all background conditions including land, sea, even cloud. Guan et al. (2010) have shown how the AI is used strategically for smoke-plume analyses. A-Train radar and lidar data used here are native 94 GHz reflectivity and attenuated 532 nm attenuated backscatter, respectively, as described in Mace et al. (2006) and Vaughan et al. (2004).

Fig. 1. Map of the fire zone and environs, with place names mentioned in the text. Black polygons are final burnt perimeter for the Wollemi and Grose Valley fires. Red polygons are scars mapped from LandSat imagery from 7 January 2007. Green enclosure: National Park boundary. Light brown: elevation > 800 m MSL. Grey: urban areas.

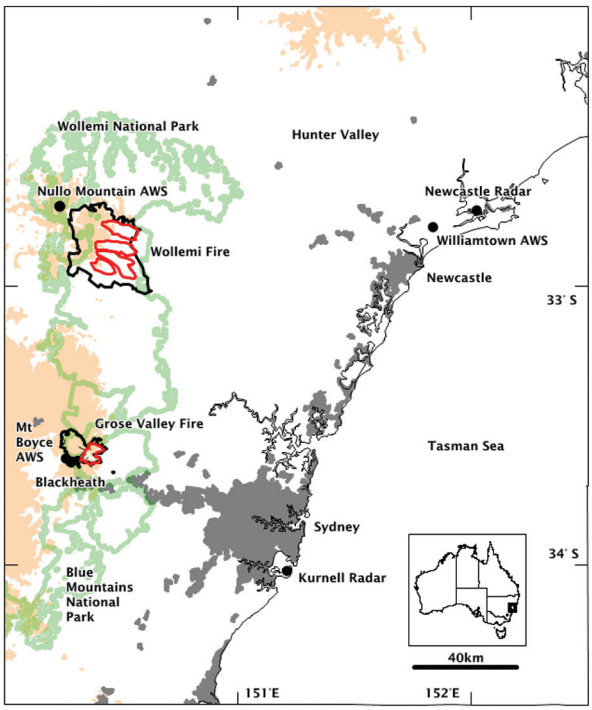

Weather radar

Weather radar data from Newcastle (32.73°S, 152.03°E), provided by Australia's Bureau of Meteorology, are used to calculate echo-top altitude. Level two reflectivity data forming a full volume scan are available at 10-minute resolution. Range resolution is 1 km; azimuthal resolution is 1°. Vertical sampling is determined by elevation angle and target distance. For instance, at 100 (150) km range, the vertical pixel spacing between adjacent scan angles is approximately 2.0 (2.3) km at upper troposphere altitudes. Echo-top altitude is the pixel-center altitude at the top of a column of contiguous echoes all exceeding +5 dBZ.

Weather data and analyses

We use radiosonde temperature, humidity and tropopause data at Williamtown (32.8°S, 151.83°E, ~120 km east of Wollemi, 160 km northeast of Grose Valley). Soundings were performed only at 0000 UTC each day. Surface hourly data are from Mt. Boyce (33.6°S, 150.3°E) and Nullo Mountain (32.7°S, 150.2°E) automated weather station (AWS) sites close to but upwind of the Grose Valley and Wollemi fires, respectively.

Analysis

Pyroconvection views from space and ground

The particular fires under study are known as the Grose Valley and Wollemi fires. The Grose Valley fire (approximate point of origin, 33.5°S, 150.3°E) began as two separate fires in the Blue Mountains National Park, ignited by lightning on 13 November (Cronstedt, 2007). The Wollemi fire (approximate point of origin, 32.8°S, 150.4°E) started 13 November in the Wollemi National Park (Price, 2010). These fires were roughly 75 km apart and co-oriented approximately north-south (Fig. 1). Both fires were active into the first week of December, when they were brought into final containment (Cronstedt, 2007). On 22 November, and only on that date, both fires experienced pyrocumulonimbus (pyroCb) blow ups. Cronstedt (2007) identified 22 November as a unique day in the life of the Grose Valley fire behavior and fire weather. That paper also reported observed column development to 6 km. Here we will confirm the pyroCb and extend its injection height estimate considerably. Figure 2 contains a photograph of the Grose Valley pyroCb column from Blackheath (approximately 5 km southwest) taken at ~0300 UTC. Note the column top punching into a glaciated cloud and a lower turret in the foreground with a pileus cap, both signs of vigorous convection reaching to ice-formation altitudes.

Satellite views

22 November

NASA's A-Train fleet of platforms passed directly over the fire zone at ~0400 UTC 22 November. Figure 3 contains a true colour image from Aqua MODIS and fire perimeters.

Fig. 2. Photograph of active Grose Valley pyrocumulonimbus on 22 November 2006, taken from Blackheath, ~5 km southwest of the fire, ~0300 UTC. Credit: Lindsay Pearce, http://www.blackheathweather.com/

Fig. 3. Aqua MODIS true colour and fire perimeter (orange polygons), 0355 UTC 22 November. Wollemi fire (center, top) and pyroCb anvil; Grose Valley fire (center, bottom) and low smoke plume. Downwind of plume, high ice clouds. Three-hour back trajectories launched at 0400 UTC, at location of local maxima of OMI aerosol index (see text for details). See legend for trajectory launch altitudes (MSL). Black line: CALIOP/CloudSat track (see Fig. 6). Google Earth projection.

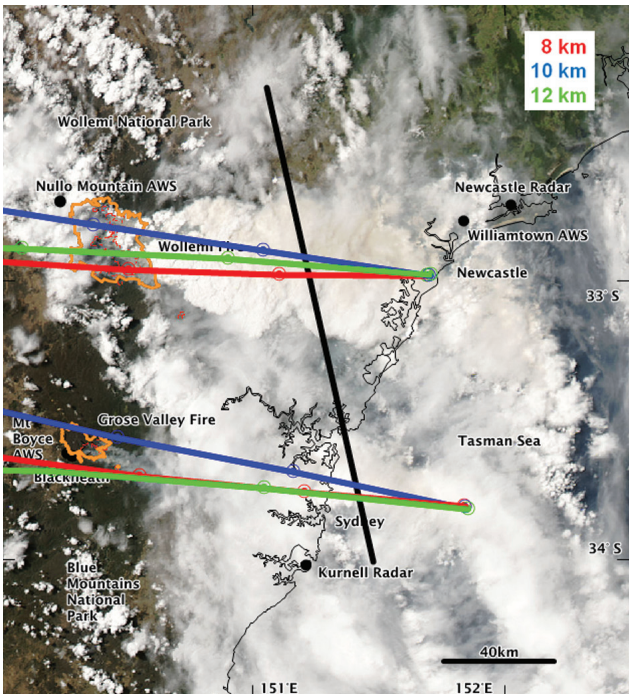

The Wollemi and Grose Valley fires, and considerable cloud cover east of the fires, are evident. The Wollemi fire is in the state of active pyrocumulonimbus convection—an anvil is 'connected' to the fire (and most likely obscuring parts of the fire). There appear to be two separate streams of pyroconvective cloud east of the Wollemi fire complex; to the south a single, relatively long anvil cloud and a broken stream of convective clouds to the north. The anvil spreads east, and consists of a highly textured cloud closest to the fire, and a cloud with apparent glaciation further downwind. The MODIS 11μm brightness temperature (BT) minimum in the Wollemi anvil is -60 °C. Relating this cloud-top temperature to height (Fig. 4) using the nearest radiosonde (Williamtown) at 0000 UTC gives a pyroCb column height of approximately 12.2 km, within ~200 m of the cold-point tropopause (12.4 km, 190 hPa). There is tannish colouration over the downwind portions of the anvil, indicating a considerable abundance of smoke at or above the cloud top. The sky just east of the Grose Valley fire is cloud free, revealing two closely situated smoke plumes emitted by the fire complex. East of these plumes is an overcast of cloud with glaciated appearance. The trajectory paths overplotted in Fig. 3 will be discussed later.

Figure 5 is a plan view of the fire and plume area containing two A-Train image products. The yellow contours enclose areas with Aqua MODIS BT < -45 °C. There are two relatively large contoured areas, one east of the Wollemi fire and spreading nearly to the sea coast. The other is offshore, north of the 34°S parallel. Colour-shaded pixels represent level two OMI AI. The AI features indicate smoke. Smoke covers the two largest contoured areas described above. The positive AI signals confirm the presence of absorbing aerosols even in the presence of the optically thick clouds

Fig. 4. Skew-T log p diagram with 0000 UTC radiosonde temperature and dewpoint temperature data from Williamtown. Red solid line; 22 November. Black solid; 21 November. Black dotted; 20 November (all 2006).

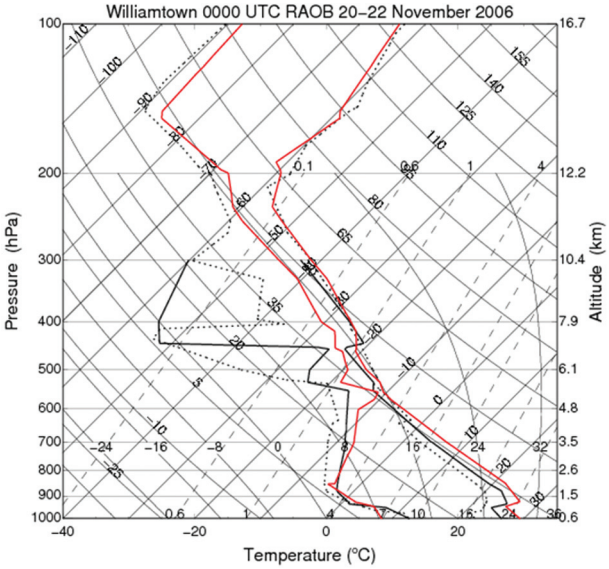

represented here by the -45 ˚C contours, and in Fig. 3 as optically opaque. Thick clouds obscure underlying UV-backscattering layers (Penning de Vries and Wagner, 2011), hence the enhanced AI here means the smoke is mixed with or situated above deep, opaque cloud tops. Double-digit AI values have been shown to be indicative of optically dense, high-altitude smoke plumes (Guan et al., 2010; Fromm et al., 2010). Hence the OMI AI and MODIS visible plus MODIS BT together indicate a substantial mass of smoke aerosols in the uppermost troposphere and tropopause region, injected by the Wollemi pyroCb. To the south, there is yet another—albeit weaker—AI feature that is distinct from the Wollemi plume. This AI feature is also situated where MODIS BT < -45 ˚C. Thus even though the AI signal is relatively weak, it is a robust indicator of absorbing aerosols at or above an optically thick, high-altitude ice cloud. We explore the source of those aerosols next.

Figure 3 contains paths from two groups of back trajectories. The initiation point corresponds to the location and time of the two localised OMI AI maxima. Examining

Fig. 5. OMI Aerosol Index, colour-scaled between 1–11.25. Asterisks give fire location. Yellow contour is MODIS 11μm BT = -45 ˚C. Start points for trajectories shown in Fig. 3 at head of white arrows, near core of each AI-plume feature.

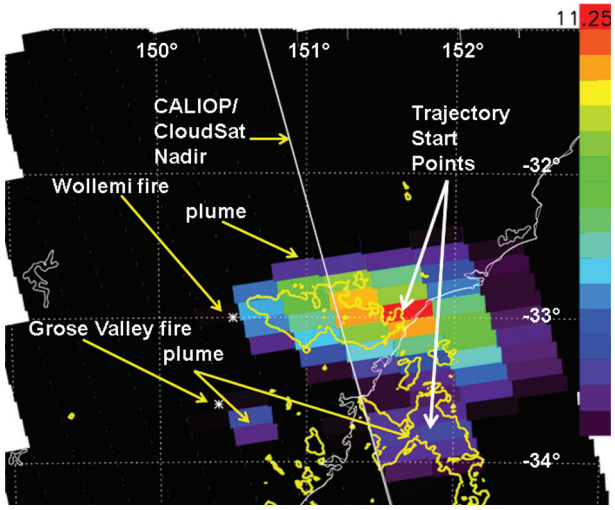

Fig. 6. CloudSat reflectivity (blue–white scale) and CALIOP 532 nm attenuated backscatter (black–white scale), ~0400 UTC 22 November 2006, through Wollemi pyroCb anvil (~32.9˚S) and Grose Valley pyroCb blow-off (~33.8˚S), annotated for convenient reference. CALIOP data plotted last. Red line, OMI AI co-located along lidar/radar nadir (scale on right axis). Black dashed line: lifting condensation level (LCL) according to 0000 UTC Williamtown radiosounding. Black, vertical arrow: cloud-break area discussed in text.

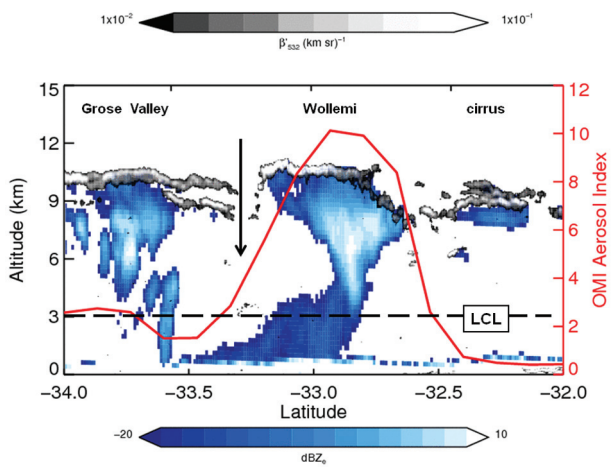

Fig. 7. OMI Aerosol Index map, ~0300 UTC 23 November 2006, colour-scaled between 1–5.59. Yellow arrows point out features of focus, as annotated.

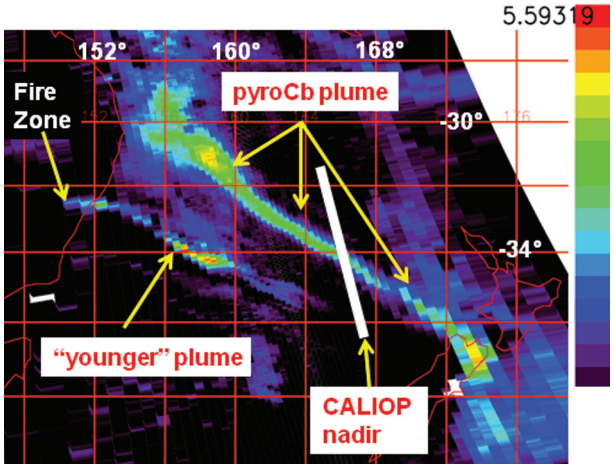

Fig. 8. CALIOP 532 nm attenuated backscatter, ~0300 UTC 23 November 2006 (see Fig. 7 for plan view of the curtain). White line, OMI AI co-located along lidar/radar nadir (scale on right axis). Yellow arrows outline smoke plume; black arrows point to cloud. Black box marks meridional extent of AI larger than noise threshold.

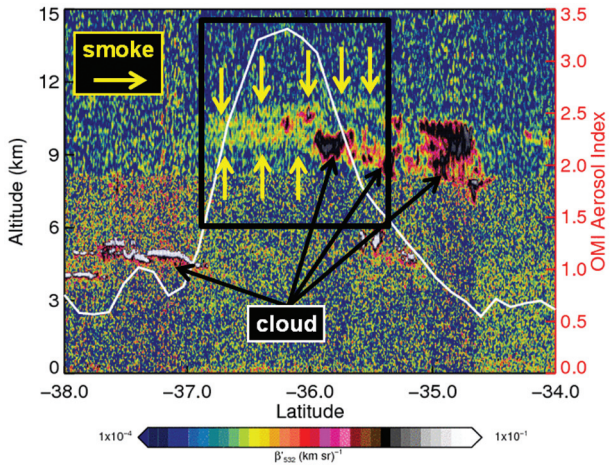

Figs. 3 and 5, we see that the smoke is sufficiently strong on/over the Wollemi anvil to impact the cloud's colour. This is not readily apparent near the southern AI maximum, which is consistent with the much smaller AI maximum there—i.e. the smoke is optically thinner in the southern plume situated at or above cold cloud tops. The MODIS BTs then give us the rationale for launching both sets of trajectories from the same altitude range to assess the origin of the smoke. Hybrid Single-Particle Lagrangian Integrated Trajectory Model (HYSPLIT) (Draxler and Rolph, 2010) trajectories were run for three hours (0400 to 0100 UTC) at 8, 10, and 12 km ASL. The northern (southern) set of trajectories pass close to the Wollemi (Grose Valley) fire, between roughly 0100–0200 UTC, suggesting that each high-altitude plume was injected two to three hours before the A-Train observations, i.e. between roughly 11.00 am and 12.00 pm local standard time. This is an unusually early time for mature pyroconvection (Fromm et al., 2010). It is also interesting to note the implication that two separate fires blew up at this early time.

We get detailed insights from space-based radar and lidar regarding the top and internal structure of the Wollemi and Grose Valley pyroCb clouds. Figures 3 and 5 show the location of the CALIOP and CloudSat slices through the clouds generated by these blow ups. These active sensors sample both AI features and the accompanying deep, optically thick water-ice cloud. Figure 6 presents the OMI AI, lidar and radar views through this slice. The pyroclouds in Fig. 6 are labeled for ease of reference. This is the first reported analysis of pyroCb-generated clouds using active instruments that penetrate the cloud boundaries and allow a critical look at the internal structure. At the visible lidar wavelength, backscatter from hydrometeors is most sensitive to the integrated cross-sectional area of the scatterers, whereas at the radar wavelength the echoes are most sensitive to the integrated volume of the scatterers. Therefore, these data indicate that the cloud tops between 9 and 11 km associated with the enhanced AI have an increased number of smaller particles in the areas where lidar backscatter is large (~ 1×10^{-1} sr^{-1} km^{-1}) and the radar reflectivity is small (~ -20 dBZ_e).

The Wollemi anvil (Fig. 6) penetrates demonstrably close to the tropopause, is convective in nature, has positive AI, and exhibits distinctively large echo intensity above the lifting condensation level (LCL) determined from the Williamtown radiosonde profile at 0000 UTC. A wedge of weak echoes broadens from near the base of the convective cloud southward and downward. At the surface this feature is continuous between ~32.9˚ and 33.5˚S. The scattering particles here are unlikely to be precipitation considering that they jut out far from the base of the cloud, and that the echo intensity is much less than that of the cloud itself. A narrow portion of the low-altitude feature is exposed via a cloud break at ~33.25˚S (see black arrow in Fig. 6). Examining this area in Fig. 3 we see a small cloud gap just south of the Wollemi pyroCb cloud. Here the appearance is of a grayish, translucent cover above the ground. This seems more consistent with a smoke plume than a precipitation shield. Hence the swath of small-reflectivity echoes from the ground to the cloud base is probably an indicator of a large concentration of large smoke particles, chaff, and related debris emitted by the Wollemi fire.

The Grose Valley cloud to the south in Fig. 6 also embodies a positive AI signal. Its altitude is roughly the same as the Wollemi anvil, but it is vertically patchy and less extensive. Referring back to the nadir visible and IR views in Fig. 3 and 5, this vertical structure appears to be consistent with a cloud totally decoupled from its convective origin. It appears that the A-Train slice here discerns a cirrus cloud polluted with smoke and lower cloud elements probably in an early phase of decay from convective origin. The tropopause-level plumes from both pyroCbs are a peculiar mixture of smoke and ice crystals. The curious cloud microphysics of this event is the subject of ongoing investigation and beyond the scope of this paper.

23 November

OMI AI and CALIOP backscatter are also strategic for identifying the Wollemi and Grose Valley smoke plumes the day after the pyroCbs. Figure 7 shows a map centered on the Tasman Sea, displaying the OMI AI on 23 November at ~0300 UTC. A long, narrow smoke plume stretches from Australia southeast across the sea to New Zealand. There is a second, smaller plume situated closer to Australia that is likely a marker of later fire activity. The CALIOP path reveals where the lidar swept through the longer smoke plume, near 34˚S, 166˚E.

Figure 8 is constructed similarly to Fig. 6, but without CloudSat data. The co-located CALIOP backscatter and OMI AI reveal an area between ~35.3˚ and 37.0˚S of absorbing aerosols. The backscatter curtain indicates relatively strong scattering layers consistent with cirrus clouds between 8–10 km near the area of enhanced AI. However, there is also a weaker scattering feature precisely encompassing the enhanced AI swath. The yellow arrows in Fig. 8 surround this feature, which is at an altitude that in some parts is higher than the cirrus cloud. Again, absorbing aerosols below thick cloud cannot be detected by OMI, so the continuous swath of positive AI indicates a smoke layer at and above any ice clouds. We conclude that this is a smoke layer and it extends from 9–11 km. Back trajectories (not shown) confirm a path back to the fire zone at a time close to the prior day's pyroCbs. The altitude of the smoke on 23 November is also in agreement with the plume heights analysed in the previous section.

Ground-based radar

Radars at both Sydney (Kurnell) and Newcastle have a range that covers both fires' plumes but Newcastle was closest to Wollemi, the larger blow up of the two, so we focus our analysis on these data. Figure 9 gives an example of the echoes from the Wollemi pyroconvection. The time chosen, 0400 UTC, is five minutes after the A-Train encounter. Figure

9(a) shows column-summed reflectivity, to summarise the entire three-dimensional plume. We see echoes connected to the fire and spreading ~100 km eastward. Echo-tops (Fig. 9(b)) greater than 7 km extend for roughly 50 km, and are as high as ~14 km near the fire. The RHI scan in Fig. 9(c), sampling the high-echo region, confirms the strong echoes as high as 14 km. Next we analyse echo-top time series for both fires.

Fig. 9. Newcastle radar output for 0400 UTC 22 November. (a) plan-position-indicator (PPI) column-integrated reflectivity.; (b) PPI echo-tops, in km; (c) range-height indicator (RHI) of reflectivity (dBZ). The RHI view is at azimuth angle 259°, as indicated by the radial line on (a) and (b). Range ring spacing is 50 km. Wollemi and Grose Valley fire locations marked by black dots.

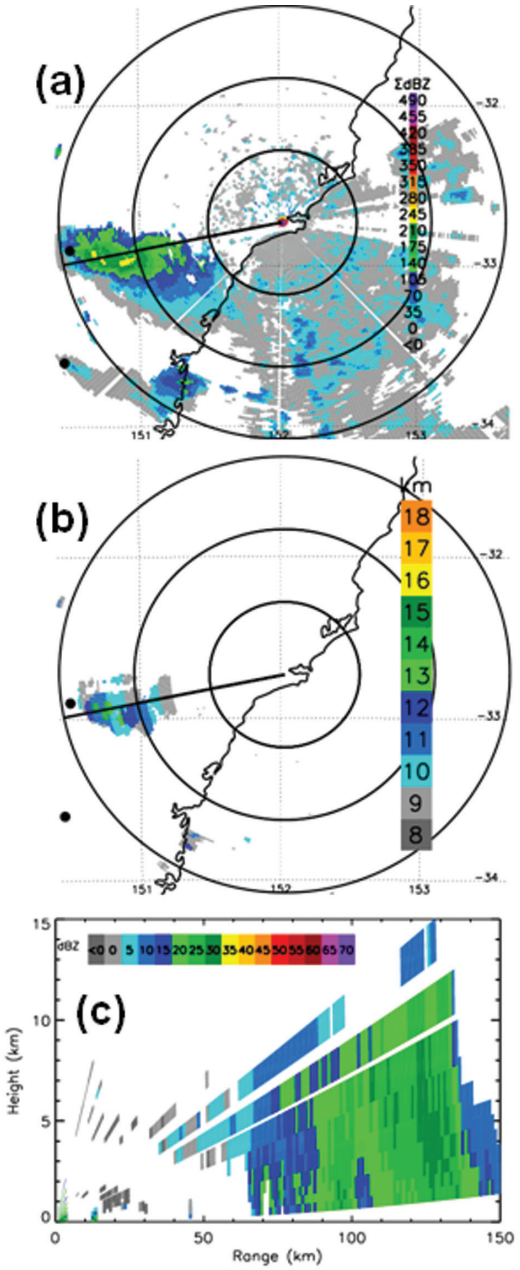

Echo-top calculations for each fire are determined by subsetting the Newcastle scans by azimuth and range to selectively sample each fire's pyroconvective column. Figure 10 shows a time series of echo-top altitude for each fire's column between 0000 and 0500 UTC 22 November. The Wollemi plume grows from ~4 km altitude at 0000 UTC to the tropopause by ~0150 UTC. The timeline indicates pulses of pyroconvection at 0050, 0140, 0230, and 0400 UTC, each involving a deeper pyroconvection injection, the 0140 and 0230 UTC pulses hitting the tropopause, and the latest clearly jutting to 14 km, above the local tropopause, even the cold-point. The Grose Valley pyroconvection initiates soon after 0100 UTC, reaches 9 km by 0150 UTC, and broaches the tropopause by 0220 UTC. The CALIOP/CloudSat pyroconvective cloud top altitude is consistent with the echo-tops preceding the A-Train sampling by 1–2 hours, when the trajectories in Fig. 3 indicate those clouds were formed. The higher echo-tops just after A-Train time suggest that the Wollemi pyroconvective plume's maximum injection height was 1–4 km higher than the evidence in Fig. 6.

Fire and weather chronology

Fire weather conditions from 15–24 November are illustrated in Fig. 11. Radiosonde measurements from Williamtown are used. Here we show the 'Continuous Haines Index' (Mills and McCaw, 2010). The so-called 'C-Haines' is an index based on the original Lower Atmospheric Severity Index (LASI) developed by Haines (1988), but which provides a continuous grade and maximum value sensitive to the most extreme fire weather conditions. C-Haines was large on 15 November, when the Wollemi and Grose Valley fires were young and growing. Then fire weather conditions moderated for two days before increasing to very large C-Haines values on 20–22 November. According to Mills and McCaw (2010), whose study of atmospheric stability related to fire weather included details of the Blue Mountains situation in November 2006, a statistical profile of summertime C-Haines near Wollemi is such that the 95th percentile value is 9.8. (The maximum possible C-Haines is ~13.) The 9.8 line in Fig. 11 reveals that only on 20–22 November did C-Haines exceed this restrictive value. Thereafter (after a cold front passage) fire weather again moderated.

Figure 11 also shows the components of C-Haines, the stability term (labeled 'CA') and humidity term ('CB'). The reader is referred to Mills and McCaw (2010) for details. The two terms are roughly equal on 20–22 November, but both terms and C-Haines reach maximum on 22 November. The temperature and humidity inputs to the C-Haines terms are shown in Fig. 12. We see that the peak of C-Haines on 22 November is accompanied by only one unique metric, a strong local maximum in 850 hPa T. Neither 700 hPa T nor 850 hPa T_d on 22 November exhibit a similarly strong inflection that would be associated with worse fire weather. Referring back to Fig. 4, we see a similarly deep well-mixed layer with nearly dry adiabatic conditions to just above 600 hPa on both 21 and 22 November. From 600–300 hPa, the environmental

Fig. 10. Echo-top time series, 0000–0500 UTC 22 November 2006. Radar source: Newcastle. Echo tops from Grose Valley (blue line) and Wollemi (red line) pyroconvection. A-Train overpass time, vertical dotted line. Lapse rate and cold-point tropopause determined from Williamtown radiosonde measurement at 0000 UTC (horizontal dotted lines).

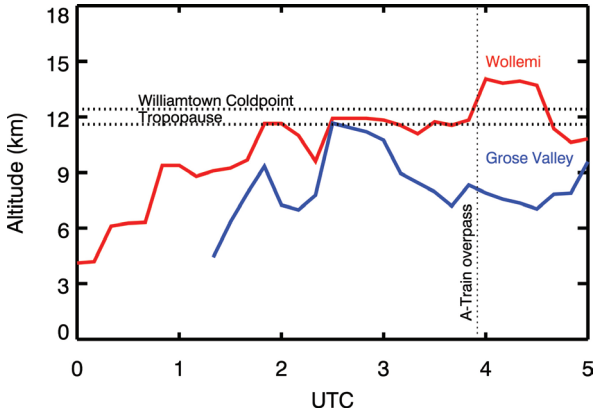

Fig. 11. Continuous Haines Index (solid black line) calculated from Williamtown radiosonde observations at 0000 UTC 15–24 November 2006. The stability term of C-Haines (dashed) and the humidity term (dash-dot) are also plotted. The grey line labeled '95%' is the 95th percentile of C-Haines for Wollemi (Mills and McCaw, 2010).

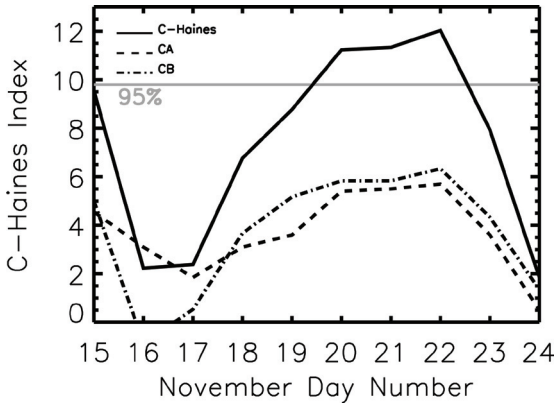

Fig. 12. C-Haines components (see plot legends) from Williamtown radiosonde observations at 0000 UTC 15–24 November 2006.

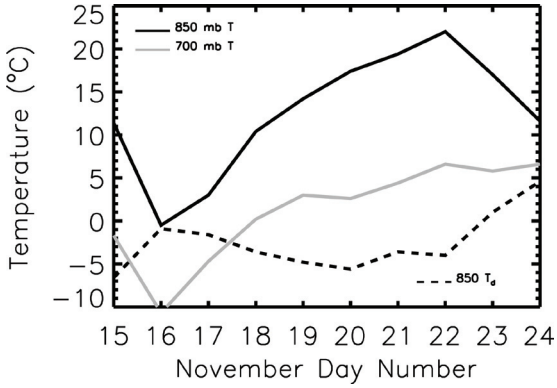

Fig. 13. Three-hour forward trajectories launched 1000 m AGL at location of Grose Valley and Wollemi fires. Start time is 0000 UTC on 20–22 November 2006 (annotated on map).

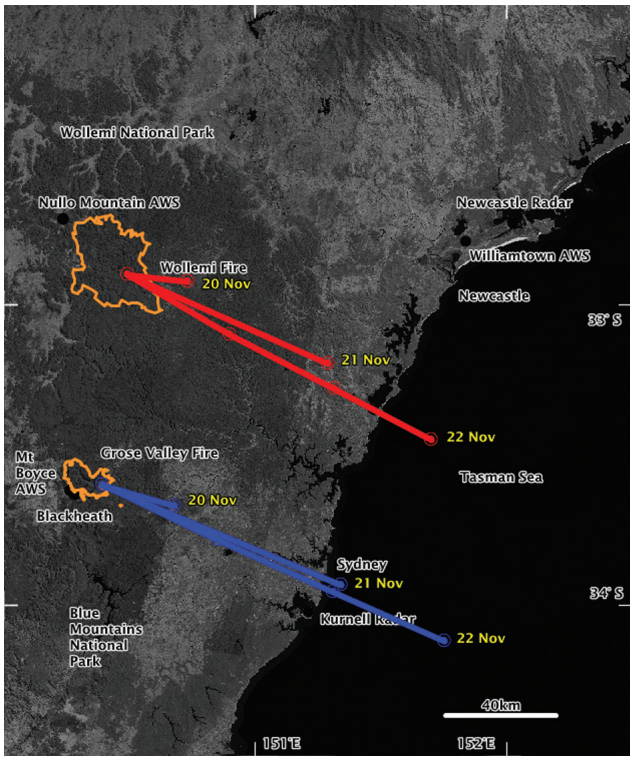

Fig. 14. Nullo Mountain and Mt. Boyce AWS FFDI components, for 0000 UTC 21–24 November 2006. Dry-bulb and dewpoint temperature (labeled 'T' 'T_d' respectively) are red lines. Sustained wind speed is plotted as blue solid lines. Ten-minute peak wind gust (not an FFDI component) is plotted identically; annotations for each wind measure are provided for clarification. Black vertical lines indicate the times of individual pyroCb blow up pulses for Wollemi (on the Nullo Mountain panel) and Grose Valley (lower panel) fires.

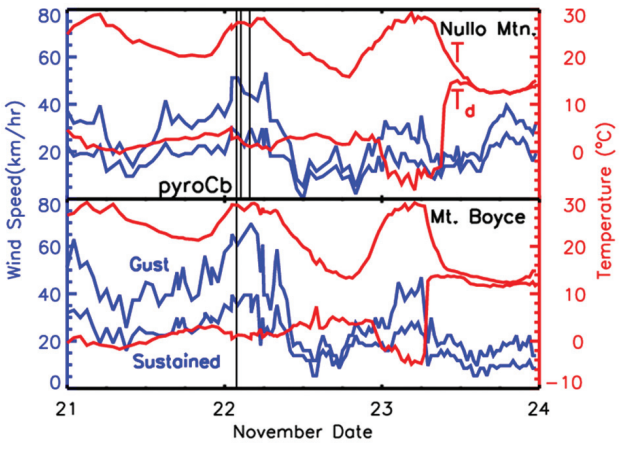

temperature profile is slightly more stable on 22 November compared to the prior day. Hence the greatest distinction of the setup conditions on 22 November is embodied in the generally warmer mixed layer just above the near-surface inversion. Both components of C-Haines are proportional to 850 hPa T; hence the consequently large 850 hPa $T–T_d$ on 22 November (Fig. 12) is primarily attributable to the increase of the dry-bulb temperature. Consequently 22 November stands out as the most extreme fire weather day. To the extent that C-Haines has skill in quantifying dangerous fire weather, we find that the peculiarly extreme conditions on 22 November were predominantly the result of an increase in sensible heat 1–3 km above the surface.

We investigated another mid-troposphere moisture condition correlated with severe bushfire, a strong water vapor gradient (termed a 'dry band,' or 'dry slot') over the fire (Mills, 2008). Hourly water vapor imagery from the geostationary Multi-functional Transport Satellite (MTSAT) was examined (not shown), between 0000 and 0400 UTC 22 November. There was no evidence of a strong dry band over any portion of New South Wales. Considerable cloud cover over the fire zone encumbered the view of water vapor features. Thus we can only conclude that there is little synoptic scale evidence of a dry band in the general vicinity of the Wollemi and Grose Valley fires prior to and during pyroconvection.

In addition to heat and moisture, wind is a well-established fire weather factor (Dowdy et al., 2009; Sharples et al., 2009). We explore the local, elevated wind conditions in Fig. 13. Plotted are three-hour forward trajectories calculated with HYSPLIT. The trajectories were launched at 0000 UTC on 20, 21, and 22 November at coordinates close to the Wollemi and Grose Valley fires, at an altitude 1000 m AGL. The trajectory paths illustrate the daily change wind speed and direction. There is no appreciable directional change, however 22 November stands out, with the greatest wind speed. Thus it appears that both fire zones experienced particularly strong wind on 22 November, above the surface but within the planetary boundary layer.

Fig. 15. MSL pressure/front/airmass analysis, 1200 UTC 21–22 November 2006. Credit: Bureau of Meteorology. (a) 1200 UTC 21 November, (b) 1800 UTC 21 November, (c) 0000 UTC 22 November, (d) 0600 UTC 22 November, (e) 1200 UTC 22 November.

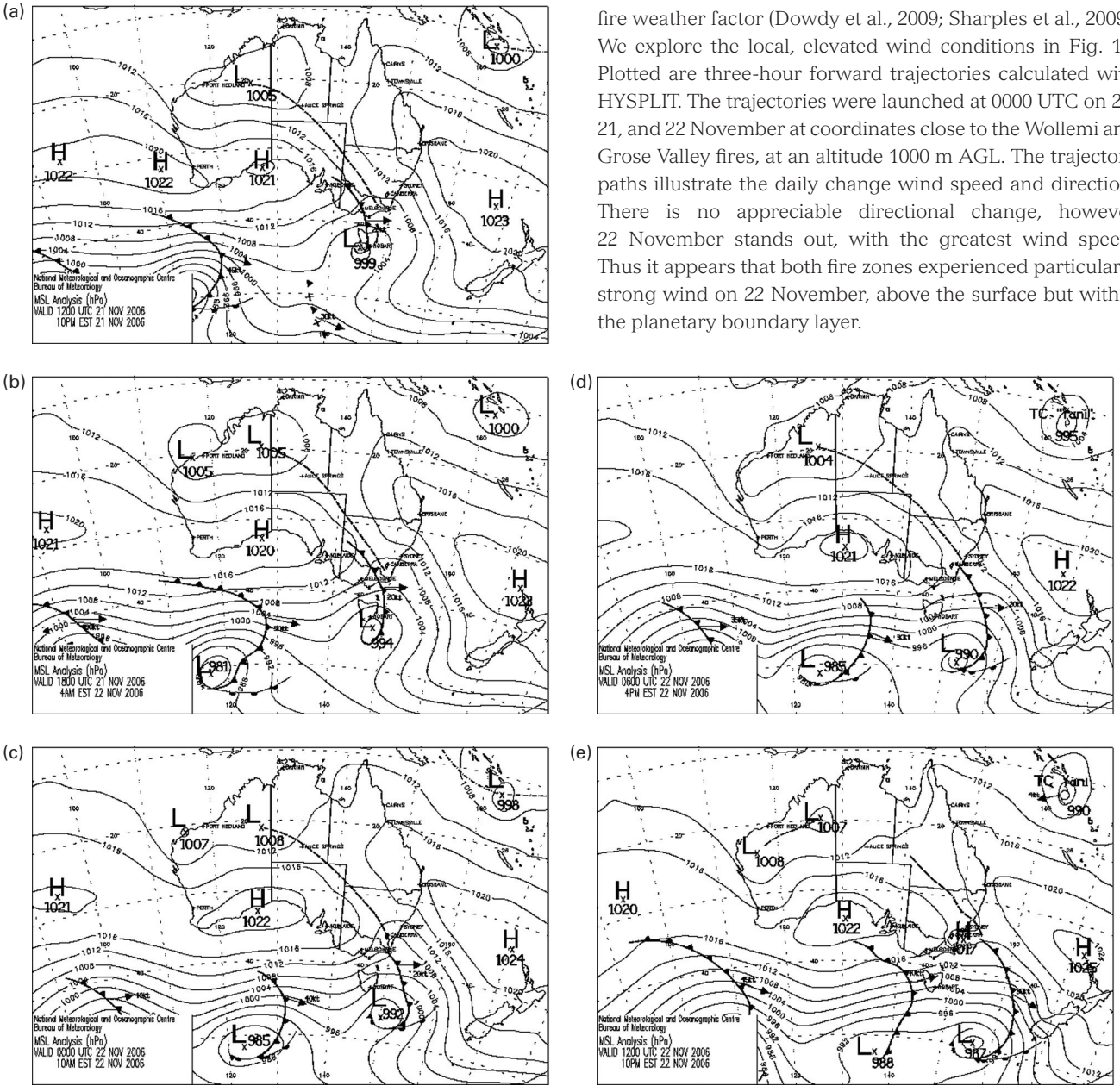

We focus now on surface fire weather conditions between 21 and 23 November—the pyroCb and two bracketing days—to assess factors associated with the pyroCbs. Cronstedt (2007) calculated the Forest Fire Danger Index (FFDI) (Noble et al., 1980) at Mt. Boyce and Nullo Mountain AWS for the life of Grose Valley and Wollemi fires. The largest FFDI at Mt. Boyce (Nullo Mountain) was 39.5 (38.6), in the class of 'very high' danger. Given that there are three greater fire danger classes of FFDI, these peak values might be considered midrange between 'low to moderate' and 'catastrophic,' yet deep pyroconvection occurred. Hence we will analyse the meteorological components of FFDI to gain insight.

Figure 14 shows the AWS hourly observations of temperature, dewpoint, and wind speed for 21–24 November (UTC). Maximum dry-bulb temperature is remarkably similar between stations and from day-to-day, varying between 28–30 °C. Dewpoint temperature at the time of diurnal maximum temperature (T_{max}) is approximately the same on 21 and 22 November, implying a similar relative humidity (RH) for both fire areas on these days. Interestingly, dewpoints drop considerably on 23 November, giving very low RH at T_{max} time. Figure 14 also shows sustained and gust wind speed. We see that at each station, peak sustained and gust winds at T_{max} time were greatest on 22 November. It is also evident that sustained wind on 23 November is considerably weaker than on the previous two days, the primary reason peak FFDI is relatively low on this date. The peak wind activity at both stations on 22 November endured for ~6 hours (~0000–0600 UTC). Considering all these factors, the most distinguishing fire weather component is the wind speed. This is perhaps the key element in the manifestation of deep pyroconvection only on 22 November.

Surface weather analysis

Figure 15 presents MSL analyses at six-hour intervals from 1200 UTC 21–22 November. At 1200 UTC 21 November an anticyclone was situated east of the fire zone centered over the Tasman Sea. A pressure trough and cold front was situated through western Victoria, separating the aforementioned anticyclone and another centered along the coast of Western and South Australia. A substantial pressure gradient exists northeast of the cold front over the fire zone, implying a considerable synoptic scale northwesterly wind. The front and associated pressure trough advance toward the fire zone, but are still several hundred kilometres southwest of the fires at 0000 UTC 22 November, just before pyroconvection ensues. The pressure gradient weakens by 1200 UTC 22 November as the trough nears Sydney from the southwest. The trough does not cross the fire zone until sometime between 0600 and 1200, after the initial deep pyroconvection has ceased. Thus there appears to be little influence on the fire zone of the trough passage, with whatever wind shift or turbulence accompanied it. The strongest evidence for synoptic scale forcing of dangerous MSL fire conditions is in the strong pressure gradient, and concomitant winds, persisting from 21 into early 22 November. Sharples et al. (2010) have shown that this is a weather pattern associated with the onset of foehn-like winds in southeastern Australia. It is possible that the relatively elevated overnight wind speeds and temperatures seen in Fig. 14 are due to a foehn effect. This forms a mechanism for earlier than expected fire escalation of 22 November.

Discussion

In the morning hours of 22 November 2006, the going Wollemi and Grose Valley fires blew up into pyrocumulonimbus storms. Weather radar began detecting pyroconvective columns between 0000 and 0100 UTC, Wollemi being first. Columns grew throughout the morning (Fig. 10), punctuated by pulses to higher altitude, and reached the tropopause by ~0150 UTC (Wollemi) and ~0230 UTC (Grose Valley). The Wollemi pyroCb column surpassed the cold-point tropopause at ~0400 UTC, topping out at ~14 km.

The telltale clue of a young (i.e. concentrated), high-altitude smoke plume provided by the OMI AI signals on 22 November, led us to an unusual observation of smoke-polluted pyroconvective anvils over coastal New South Wales in the early afternoon. Fortunately these smokey-ice clouds were situated under the lidar and radar beams of the A-Train's CALIOP and CloudSat instruments, respectively. The nadir imagery and vertical slices through the upper tropospheric pyroconvective exhaust allowed us to uniquely identify the composition/altitude of the cloud top and expose its internal structure. It also enabled the reconciliation with the next day's more expansive plume over the Tasman Sea. However, these views from orbit required additional remote sensing to more fully characterise the lifetime and injection history of the Wollemi and Grose Valley blow ups.

Ground-based radar showed that both fires spawned pyroconvection in late morning, an unusual occurrence, and that the Wollemi pyroconvective column exceeded the heights sampled by the A-Train, and involved penetration into the lowermost stratosphere. Thus the full impact of the fires on the atmosphere was optimally obtained only by the synergistic use of ground and space-based sensors. The radar data also enabled us to align the fires' most extreme behavior with surface weather observations. These give support for the finding that the relatively early local time of the blow up was attributable to early onset of strong sustained and gusty wind conditions. However, other local forces of fire behavior such as fuel, weather and terrain factors may also give important guidance for precisely characterising fire behavior that the ground-based and space based instruments employed here cannot resolve. Fortunately, aircraft-based IR linescan data were taken of the Grose Valley fire. An in-depth analysis of all available data relevant to surface fire behaviour, providing insight into the nature of blow up events, will be the subject of future work.

Summary

On 22 November 2006, forest fires in the Blue Mountains and Wollemi National Parks exploded into an extreme manifestation of fire behavior, the pyrocumulonimbus storm. The storm tops reached and broached the local tropopause. 'Day-after' plume measurements confirmed tropopause-level injection height. Implications for surface fire behavior are that on this occasion, two separate fires generated sufficiently large energy release to create multiple pulses of tropopause-penetrating convective columns. The associated meteorological data implicate planetary boundary layer sensible heat and wind speed as the driving factors behind these blow ups, even though neither measure was individually dominant. The objective evidence of the pyroCb storms (i.e. radar echo-tops), and the concomitant severe fire weather manifested on the ground, make clear the need to localise the predictors of extreme fire behavior.

Acknowledgments

We thank Tony Bannister of the Bureau of Meteorology for the level two radar data and AWS hourly surface observations. We are also grateful to the Bureau for the MSL weather maps used herein. Bo Cai Gao, Naval Research Laboratory, assisted with processing of MODIS IR data. Radiosonde data are from http://www.esrl.noaa.gov/raobs. MSL pressure and weather-depiction maps were acquired from http://www.bom.gov.au/australia/charts/archive/index.shtml. MTSAT water vapor quick-looks were accessed from http://www.jma.go.jp/jma/jma-eng/satellite/.

References

Cronstedt, M. 2007. Report on Lawson's Long Alley Section 44. Incident Controllers Report, Available from: www.habitatadvocate.com.au/wp-content/uploads/2010/09/Lawsons_Long_Alley_Section_44_Report_20070208.pdf

Dirksen, R.J., Folkert Boersma, K., de Laat, J., Stammes, P., van der Werf, G.R., Val Martin, M. and Kelder H.M. 2009. An aerosol boomerang: Rapid around-the-world transport of smoke from the December 2006 Australian forest fires observed from space, *J. Geophys. Res., 114*, D21201, doi:10.1029/2009JD012360.

Dowdy, A., Mills, G., Finkele, K. and de Groot, W. 2009. Australian fire weather as represented by the McArthur Forest Fire Danger Index and the Canadian Forest Fire Weather Index, *CAWCR Technical Report No. 10*.

Draxler, R. and Rolph, G. 2010. HYSPLIT (HYbrid Single-Particle Lagrangian Integrated Trajectory) Model access via NOAA ARL READY Website (http://ready.arl.noaa.gov/HYSPLIT.php). NOAA Air Resources Laboratory, Silver Spring, MD.

Fromm, M., Tupper, A., Rosenfeld, D., Servranckx, R. and McRae R. 2006. Violent pyro-convective storm devastates Australia's capital and pollutes the stratosphere, *Geophys. Res. Lett., 33*, L05815, doi:10.1029/2005GL025161.

Fromm, M., Lindsey, D.T., Servranckx, R., Yue, G., Trickl, T., Sica, R., Doucet, P. and Godin-Beekmann, S. 2010. The Untold Story of Pyrocumulonimbus, *Bull. Amer. Meteor. Soc., 91*, 1193–209, doi:10.1175/2010BAMS3004.1.

Giglio, L., Descloitres, J., Justice, C.O. and Kaufman, Y. 2003. An enhanced contextual fire detection algorithm for MODIS. *Remote Sensing of Environment, 87*, 273-82. doi:10.1016/S0034-4257(03)00184-6.

Guan, H., Esswein, R., Lopez, J., Bergstrom, R., Warnock, A., Follette-Cook, M., Fromm, M. and Iraci L.T. 2010. A multi-decadal history of biomass burning plume heights, identified using aerosol index measurements, *Atmos. Chem. Phys., 10*, 6461-69, doi:10.5194/acp-10-6461-2010.

Haines, D.A. 1988. A lower atmospheric severity index for wildland fires, *National Weather Digest, 13*, 23-7.

King, M.D., Kaufman, Y.J., Menzel, W.P., and Tanré, D. 1992. Remote sensing of cloud, aerosol, and water vapor properties from the Moderate Resolution Imaging Spectrometer (MODIS). *IEEE Trans. Geosci. Remote Sens., 30*, 1-27.

Mace, G.G., Marchand, R., Zhang, Q. and Stephens, G. 2007. Global hydrometeor occurrence as observed by CloudSat: Initial observations from summer 2006, *Geophys. Res. Lett., 34*, L09808, doi:10.1029/2006GL029017.

Mills, G.A. 2008. Abrupt surface drying and fire weather Part 2: a preliminary synoptic climatology in the forested areas of southern Australia, *Aust. Meteorol. Mag., 57*, 311-28.

Mills, G.A. and McCaw L. 2010. Atmospheric Stability Environments and Fire Weather in Australia – extending the Haines Index, *CAWCR Technical Report No. 20*.

Noble, I.R., Bary, G.A.V. and Gill, A.M. 1980. McArthur's fire-danger meters expressed as equations. *Aust. J. Ecol., 5*, 201-3.

Penning de Vries, M. and Wagner, T. 2011. Modelled and measured effects of clouds on UV Aerosol Indices on a local, regional, and global scale, *Atmos. Chem. Phys., 11*, 12715-35, doi:10.5194/acp-11-12715-2011.

Price, O. 2010. Developing protocols to improve early intervention in remote fires: Ignition patters in the Greater Blue Mountains World Heritage Area 1997-2007 and case study in Wollemi National Park 2006, Report to Department of Environment Climate Change and Water, University of Wollongong.

Sharples, J.J., McRae, R.H.D., Weber, R.O. and Gill, A.M. 2009. A simple index for assessing fire danger rating, *Environmental Modelling and Software, 24*, 764-74.

Sharples, J.J., Mills, G., McRae, R.H.D. and Weber, R.O. 2010. Foehn-like winds and elevated fire danger conditions in southeastern Australia, *J. Appl. Meteor. Climatol., 49*, 6, 1067-95, doi:10.1175/2010JAMC2219.1

Stephens, G., et al. 2002. The CloudSat Mission and the A-Train, *Bull. Am. Meteorol. Soc.*, 771-1790.

Torres, O., Tanskanen, A., Veihelmann, B., Ahn, C., Braak, R., Bhartia, P.K., Veefkind, P. and Levelt, P. 2007. Aerosols and surface UV products from Ozone Monitoring Instrument observations: An overview, *J. Geophys. Res., 112*, D24S47, doi:10.1029/2007JD008809.

Vaughan, M. et al. 2004. Fully automated analysis of space-based lidar data: An overview of the CALIPSO retrieval algorithms and data products. *Proc. of SPIE*. 5575.